

Supplementary Information

Effect of COFs' Linkage Isomerism on Photocatalytic Hydrogen Evolution Performance

Mingcai Zhang,^a Xuan Wu,^a Yangbin Xie,^a Xiaolong Hao,^a Qinghao Wang,^a Yongqing

Zhao,^{*, a} Jincui Wu,^a Xiaobo Pan^{*, a, b}

^aState Key Laboratory of Applied Organic Chemistry (Lanzhou University), Key Laboratory of Nonferrous Metal Chemistry and Resources Utilization of Gansu Province, College of Chemistry and Chemical Engineering, Lanzhou University, Lanzhou 730000, People's Republic of China.

*Xiaobo Pan – E-mail: boxb@lzu.edu.cn. *Yongqing Zhao – E-mail: yqzhao@lzu.edu.cn.

^bNew Energy (Photovoltaic) Industry Research Center, Qinghai University, Xining 810006, People's Republic of China.

1. Materials and methods

All reagents and solvents were purchased from commercial sources and used without further purification unless otherwise specified. Tris(4-aminophenyl)amine (N-NH₂), mesitylene (1,3,5-trimethylbenzene, 98%), 1,2-dichlorobenzene (o-DCB, 99%), sodium chlorite (NaClO₂), 2-methyl-2-butene (90%) ascorbic acid (LAA) sodium L-ascorbate (LAA-Na), dihydrogen hexachloroplatinate(IV) hexahydrate (H₂PtCl₆·6H₂O) and sodium hexachloroplatinate(IV) hexahydrate (Na₂PtCl₆·6H₂O) were purchased from Energy Chemical. 1,4-Dioxane, 1-butanol acetic acid glacial, trimethylamine (TEA) and triethanolamine (TEOA) were purchased from commercial sources. 2,4,6-Tris(4-aminophenyl)triazine (Tz-NH₂), tris(4-formylphenyl)amine (N-CHO), and 4,4',4''-(1,3,5-triazine-2,4,6-triyl)tribenzaldehyde (Tz-CHO) were synthesized following reported procedures¹⁻³.

1.1 Solution nuclear magnetic resonance (NMR) spectroscopy

Liquid ¹H and ¹³C NMR of the samples dissolved in suitable deuterated solvents were recorded on a JNM-ECS 400M spectroscopy at room temperature.

1.2 Powder X-ray diffraction (PXRD)

PXRD data were collected on a MiniFlex600 (Rigaku) Bragg-Brentano geometry with a Cu K α -radiation ($\lambda=1.540593$ Å). Samples were ground and mounted onto a sample holder. PXRD patterns were collected from 3.01° to 40° with a step size of 0.02° and a scan speed of 5° min⁻¹.

1.3 Fourier-transform infrared (FT-IR) spectroscopy

The FT-IR analyses of the samples were carried on a Bruker Vertex 70 by using KBr pellet with the range of 4000-400 cm⁻¹.

1.4 Solid-state ¹³C cross-polarization magic-angle spinning (¹³C CP/MAS) NMR spectroscopy

¹³C CP/MAS NMR spectra were recorded on a AVANCE NEO 600 MHz WB FT-NMR. The sample was loaded into a 4 mm rotor, which was mounted in a standard dual resonance MAS probe.

1.5 X-ray photoelectron spectroscopy (XPS)

XPS data was carried out by Axis Supra X-ray photoelectron spectrometer. The

spectra were referenced to the adventitious C 1s peak at 284.600 eV.

1.6 Nitrogen adsorption-desorption analysis

Nitrogen sorption measurements were recorded on an ASAP2020M&TriStar3020 adsorption analyzer at 77 K. Prior to the analysis, the samples were degassed at 393 K for 12 h. The surface areas were calculated by Brunauer-Emmett-Teller (BET) method. The pore size distributions were fitted by the non-localized density functional theory (NL-DFT).

1.7 Scanning electron microscopy (SEM)

The morphologies of COFs were performed on a Hitachi S-4800 cold field emission scanning electron microscope operating at an accelerating voltage of 5.0 kV. SEM images of the powders were achieved by sticking them to sample stage with conductive glue. The sample surface was sprayed with gold by a sputter Quorum Q150T-S before characterization.

1.8 Transmission electron microscopy (TEM)

TEM images were obtained on a Tecnai F30 transmission electron microscope. Samples were prepared by dropping sonicated ethanol suspensions of materials onto copper grids.

1.9 Electron paramagnetic resonance spectroscopy (EPR)

The EPR measurements were analyzed by a Bruker ER200DSRC10/12 spectrometer at room temperature. All the light irradiations were performed with a 300 W Xe lamp.

1.10 Ultraviolet-visible (UV-Vis) absorption spectra

Solid-state diffuse reflectance UV-Vis spectra were measured on a UV/Vis/NIR Spectrometer Lambda 950+Refle (Perkin Elmer) in the range of 200-800 nm at room temperature using BaSO₄ as the optical standard. Absorption spectra were calculated from the reflectance data with the Kubelka-Munk function.

1.11 Photoluminescence (PL) spectroscopy

PL emission was measured using a photoluminescence spectrophotometer FL3-21 (Horiba) with an excitation wavelength of 365 nm at room temperature. The time-resolved fluorescence decay spectroscopy was obtained on a FLS920 (Edinburgh

Instruments). The average photoluminescence lifetime was fitted by the following equation⁴:

$$\tau = \tau_1 R_1 + \tau_2 R_2 + \tau_3 R_3$$

where τ is average decay time, τ_1 , τ_2 and τ_3 are decay times fitted with triexponential kinetics function, and R_1 , R_2 and R_3 are relative magnitudes.

1.12 Contact angle measurements

Water contact angles were measured at room temperature by photographing the process of carefully dropping 3.0 μL distilled water on the surface of material. Contact angles were calculated using the contact angle plug-in from Image-J⁵.

1.13 Photoelectrochemical measurements

Photoelectrochemical measurements were performed via a CHI 660E electrochemical workstation in 0.5 M Na_2SO_4 with a three electrodes system having material films on ITO as the working electrode, Pt plate as the counter electrode and Ag/AgCl electrode as the reference electrode. The films on ITO were prepared in two steps. Firstly, a homogeneous slurry of COFs was prepared by ultrasonically dispersing 2 mg COF powder and 0.1 mg polyvinylidene fluoride (PVDF) into 0.1 mL DMF. Then, films on ITO were prepared by drop coating 10 μL of each samples on ITO to cover 1 cm^2 area and dried completely. A Xe lamp (CEL-HXF300-T3, 300 W) fitted with a cut-off filter (≥ 420 nm) was used as the light source for measurements. The photocurrent was tested by Amperometric i-t Curve method under the irradiation of visible light. The electrochemical impedance spectroscopy (EIS) was performed at open-circuit voltage with AC amplitude of 5 mV in frequency range of 0.01 Hz to 10^5 Hz. The Mott-Schottky analysis was recorded with the frequency of 600, 800 and 1000 Hz.

1.14 Photocatalytic hydrogen evolution experiments

Photocatalytic hydrogen evolution experiments were performed in a 300 W Xe lamp (CEL-HXF300-T3). The glass light reactor was charged with 5 mg of catalyst, 25 mL water containing ascorbic acid (0.1 M) or sodium ascorbate (0.1 M) as sacrificial electron donor and 16 μL $\text{H}_2\text{PtCl}_6 \cdot 6\text{H}_2\text{O}$ (0.1 M) or $\text{Na}_2\text{PtCl}_6 \cdot 6\text{H}_2\text{O}$ (0.1 M). The resulting suspension was sonicated for 15 minutes before degassing by N_2

bubbling for 30 minutes to remove air as possible. The generated gas was detected every 1 h with a thermal conductivity detector on a gas chromatography (Varian, 450-GC, N₂ carrier) and compared to a standard gas with known concentration of hydrogen. The photocatalytic hydrogen evolution reaction rates were determined from a linear regression fit. Hydrogen dissolution in the reaction solution was not measured, and the pressure increase due to hydrogen evolution was ignored in the calculations.

1.15 Structural simulation

Molecular modeling of all COFs was generated with Material Studio 8.0^{6, 7}. The lattice models were fully optimized by Material Studio Dmol3 molecular dynamics module method. Pawley refinement was carried out using Reflex, a software package for crystal determination from PXRD patterns.

1.16 Time Dependent Density Functional Theory (TD-DFT) calculation

First, the structural units of the four materials were optimized, using B3LYP/6-31G* to optimize in Gaussian 09W⁸, and then using TD-DFT to calculate the S1 excited state.

Analysis of electrons and holes during electron excitation using Multiwfn⁹. For TD-DFT, the expressions for holes and electrons can be written as:

$$\rho^{hole}(r) = \rho_{(loc)}^{hole}(r) + \rho_{(cross)}^{hole}(r)$$

$$\rho^{ele}(r) = \rho_{(loc)}^{ele}(r) + \rho_{(cross)}^{ele}(r)$$

where \mathbf{r} is a coordinate vector.

Then, $S_m(\mathbf{r})$ and $S_r(\mathbf{r})$ are defined to describe the overlap function between electrons and holes, where $S_m(\mathbf{r})$ and $S_r(\mathbf{r})$ are two different definitions for describing the overlap, the former takes the minimum of the hole and electron and the latter takes the geometric mean:

$$S_m(r) = \min[\rho^{hole}(r), \rho^{ele}(r)]$$

$$S_r(r) = \sqrt{\rho^{hole}(r)\rho^{ele}(r)}$$

In order to facilitate the measurement and discussion of the electronic excitation characteristics through some quantitative numerical measurements, the S_m and S_r

indices, i.e., the $S_m(\mathbf{r})$ and $S_r(\mathbf{r})$ functions are defined to be integrated in full space:

$$S_m index = \int S_m(r) dr = \int \min[\rho^{hole}(r), \rho^{ele}(r)] dr$$

$$S_r index = \int S_r(r) dr = \int \sqrt{\rho^{hole}(r)\rho^{ele}(r)} dr$$

Larger values of these two indices indicate a higher degree of overlap of holes and electrons; smaller values indicate a more significant separation of holes and electrons. The value range of these two indices is [0, 1], 1 means that the holes and electrons are perfectly overlapped, and 0 means that there is no overlap at all.

In addition, the distance between the center of mass of holes and electrons is also measured by the D index:

$$D_x = |X_{ele} - X_{hole}|$$

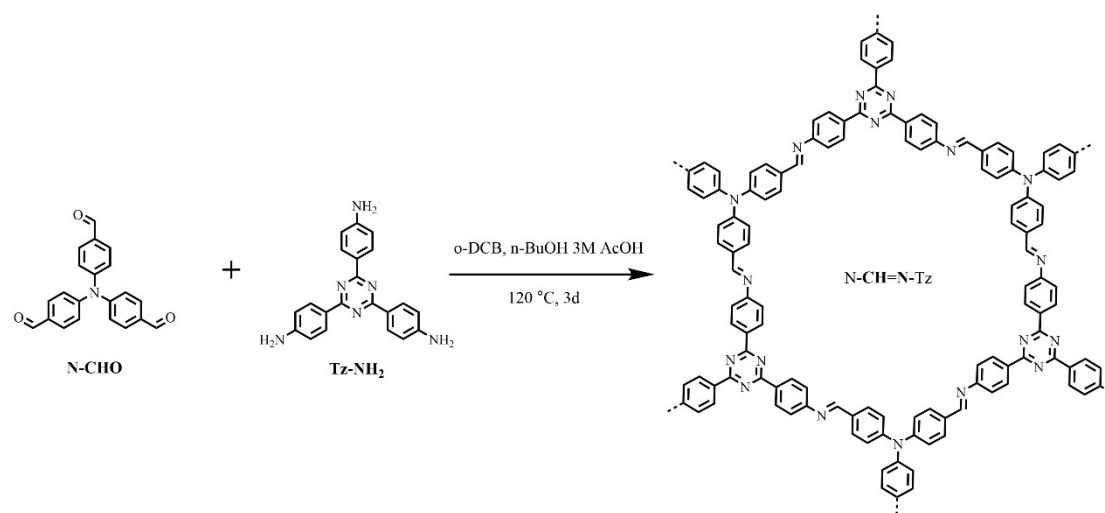
$$D_y = |Y_{ele} - Y_{hole}|$$

$$D_z = |Z_{ele} - Z_{hole}|$$

$$D index = \sqrt{(D_x)^2 + (D_y)^2 + (D_z)^2}$$

2. Synthesis of COFs

2.1 Synthesis of N-CH=N-Tz¹⁰

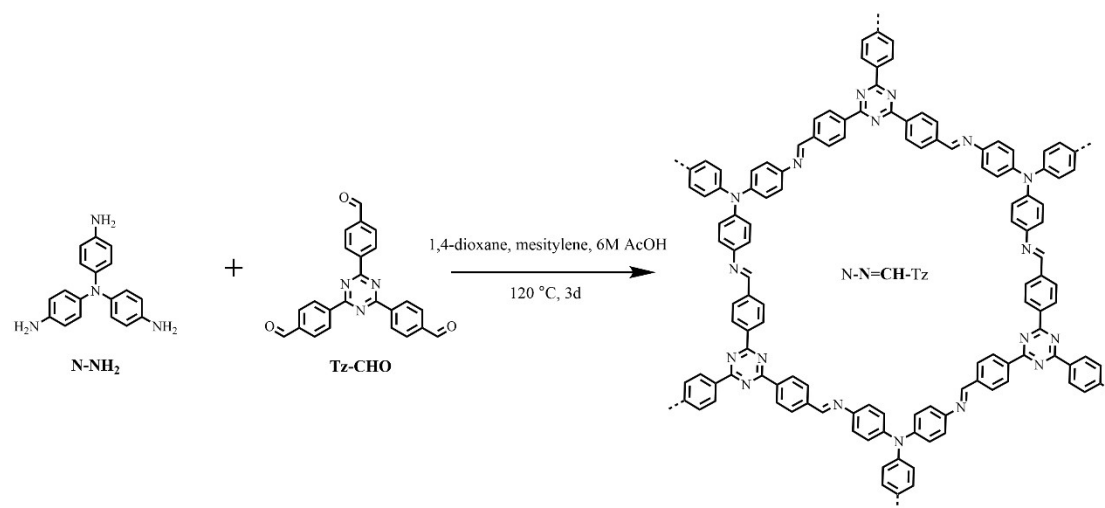


Scheme S1. Scheme of synthesis of N-CH=N-Tz.

A pyrex tube is charged with a mixture of N-CHO (0.2 mmol, 65.8 mg), Tz-NH₂ (0.2 mmol, 70.8 mg), 0.4 mL o-DCB, 0.6 mL n-BuOH and 0.2 mL of 3 M acetic acid. The mixture was sonicated for 5 min to get a homogenous dispersion. The tube was

then flash frozen at 77 K (liquid N₂ bath) and degassed by three freeze-pump-thaw cycles. The tube was sealed off and then heated at 120 °C for 3 days. A yellow colored precipitate formed was collected by filtration, washed with THF and finally Soxhlet extraction with THF for 12 h. The powder was dried at 50 °C under vacuum overnight to give the N-CH=N-Tz in an isolated yield of 70 %.

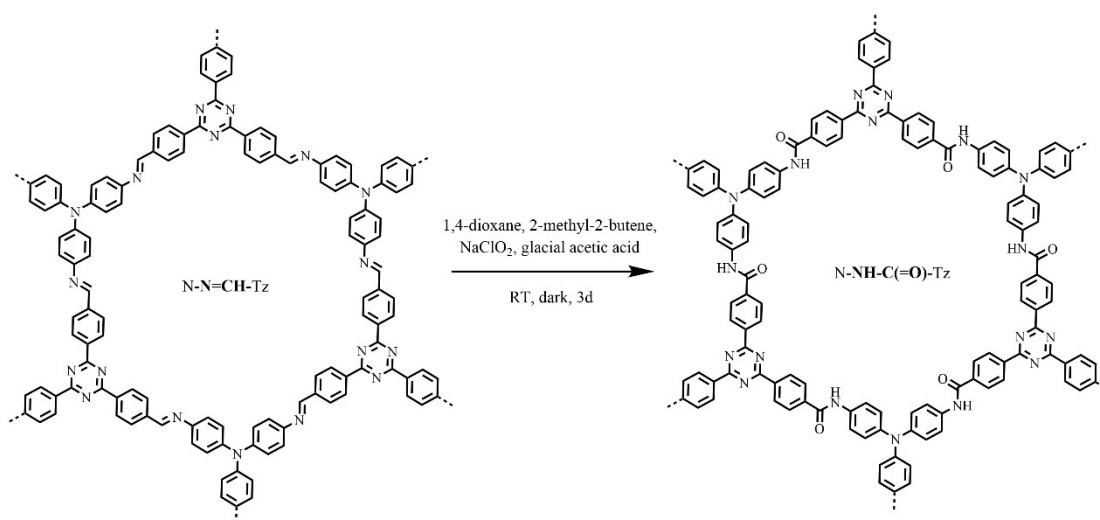
2.2 Synthesis of N-N=CH-Tz¹¹



Scheme S2. Scheme of synthesis of N-CH=N-Tz.

A pyrex tube is charged with a mixture of N-NH₂ (0.24 mmol, 70.0 mg), Tz-CHO (0.24 mmol, 94.8 mg), 5 mL 1,4-dioxane, 5 mL mesitylene and 1.2 mL of 6M acetic acid. The mixture was sonicated for 5 min to get a homogenous dispersion. The tube was then flash frozen at 77 K (liquid N₂ bath) and degassed by three freeze-pump-thaw cycles. The tube was sealed off and then heated at 120 °C for 3 days. A red colored precipitate formed was collected by filtration, washed with THF and finally Soxhlet extraction with THF for 12 h. The powder was dried at 50 °C under vacuum overnight to give the N-N=CH-Tz in an isolated yield of 78 %.

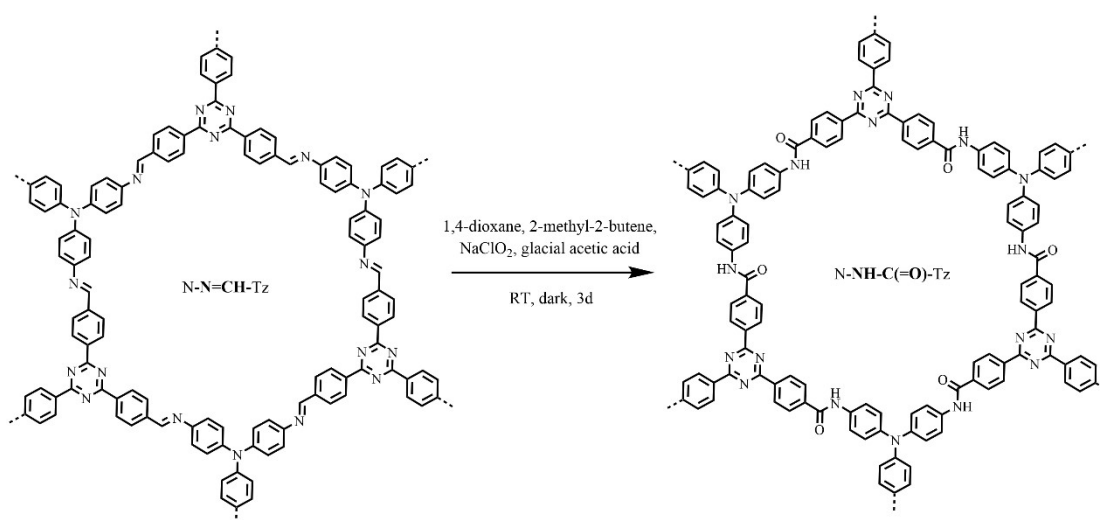
2.3 Synthesis of N-CH(=O)-NH-Tz



Scheme S3. Scheme of synthesis of N-CH(=O)-NH-Tz.

To a suspension of N-CH=N-Tz (12.7 mg, 0.06 mmol by imine) in 1,4-dioxane (1 mL) was added 2-methyl-2-butene (637 μL , 6.0 mmol, 100 eq), fresh aqueous NaClO_2 solution (100 μL , 0.33 mmol, 5.5 eq), and glacial acetic acid (34.4 μL , 0.6 mmol, 10 eq) in sequence. The biphasic suspension was let stand without stirring at room temperature in the dark for 24 h, after which an additional portion of NaClO_2 (100 μL , 0.33 mmol, 5.5 eq) was added each 24 h. N-CH(=O)-NH-Tz was isolated by filtration and washed with water, then 10 % sodium thiosulfate, then water and acetone. The material was adopted Soxhlet extraction with water/methanol (v/v=1/1) for 24 h. The powder was dried at 60 $^\circ\text{C}$ under vacuum overnight to give the N-CH(=O)-NH-Tz in an isolated yield of 55 %.

2.4 Synthesis of N-NH-C(=O)-Tz



Scheme S4. Scheme of synthesis of N-NH-(C=O)-Tz.

To a suspension of N-CH=N-Tz (12.6 mg, 0.06 mmol by imine) in 1,4-dioxane (1 mL) was added 2-methyl-2-butene (637 μ L, 6.0 mmol, 100 eq), fresh aqueous NaClO₂ solution (182 μ L, 0.6 mmol, 10 eq), and glacial acetic acid (34.4 μ L, 0.6 mmol, 10 eq) in sequence. The biphasic suspension was let stand without stirring at room temperature in the dark for 24 h, after which an additional portion of NaClO₂ (182 μ L, 0.6 mmol, 10 eq) was added each 24 h. N-NH-(C=O)-Tz was isolated by filtration and washed with water, then 10 % sodium thiosulfate, then water and acetone. The material was adopted Soxhlet extraction with water/methanol (v/v=1/1) for 24 h. The powder was dried at 60 °C under vacuum overnight to give the N-NH-(C=O)-Tz in an isolated yield of 26 %.

3. Characterizations of COFs

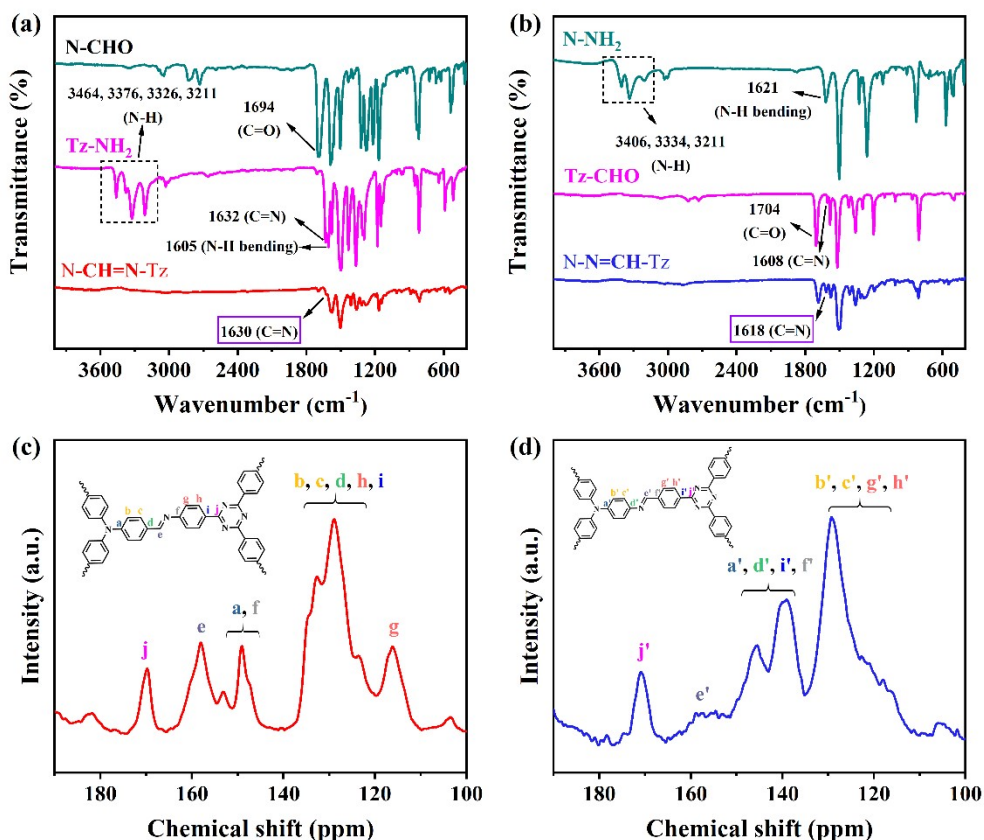


Figure S1. Structural characterization of imine-COFs. FT-IR spectra of N-CH=N-Tz (a) and N-N=CH-Tz (b). ¹³C CP/MAS ssNMR spectra of N-CH=N-Tz (c) and N-N=CH-Tz (d).

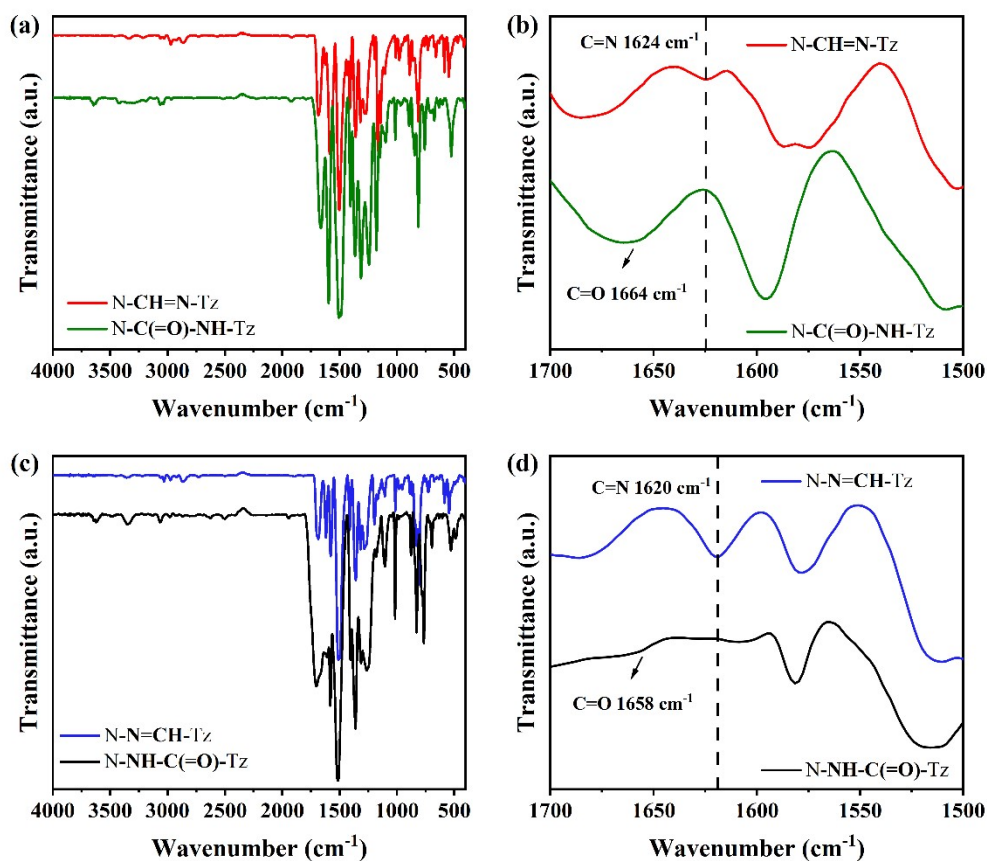


Figure S2. Structural characterization of amide materials. FT-IR spectra of N-C(=O)-NH-Tz (a, b) and N-NH-C(=O)-Tz (c, d).

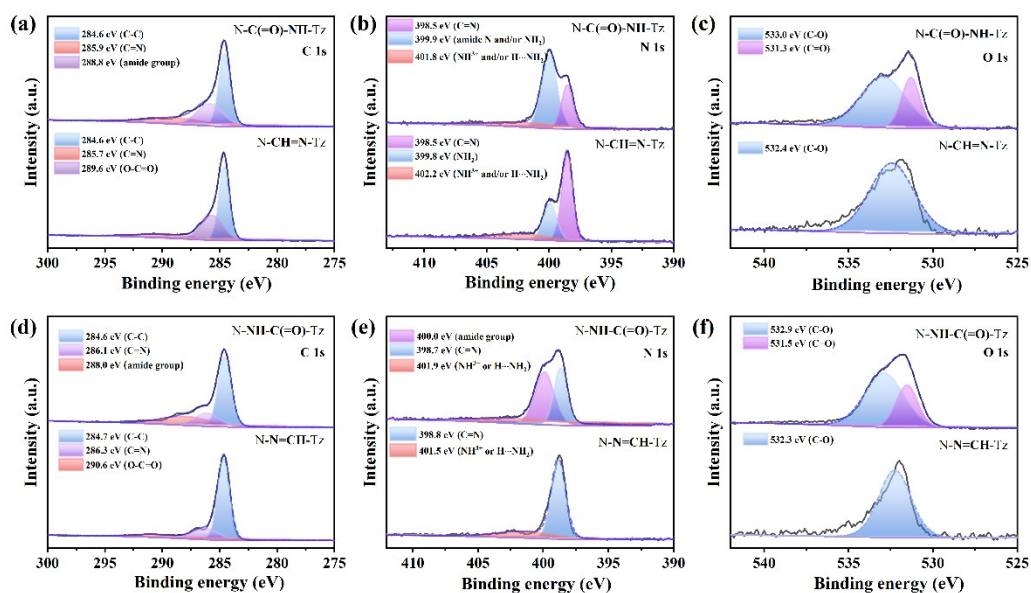


Figure S3. Structural characterization of COFs. C 1s (a), N 1s (b), O 1s (c) XPS spectra of N-CH=N-Tz and N-C(=O)-NH-Tz. C 1s (d), N 1s (e), O 1s (f) XPS spectra

of N-N=CH-Tz and N-NH-C(=O)-Tz.

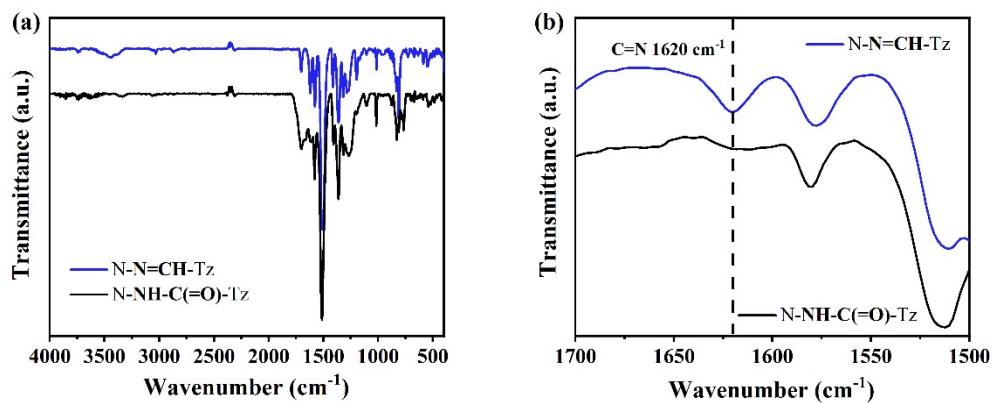


Figure S4. FT-IR spectra of N-N=CH-Tz and N-NH-C(=O)-Tz prepared at 100 μ L 3.3 M NaClO₂ solution.

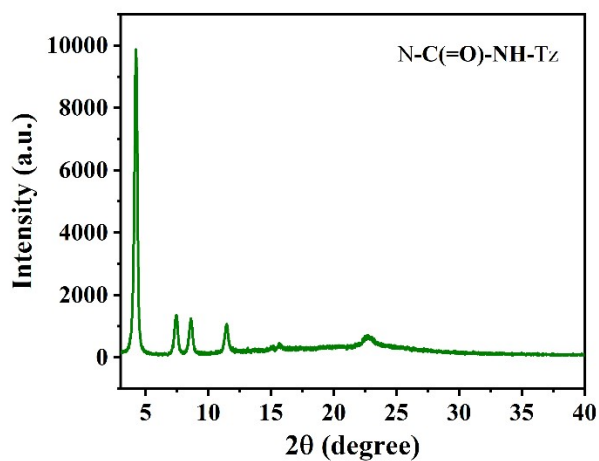


Figure S5. PXRD patterns of N-C(=O)-NH-Tz.

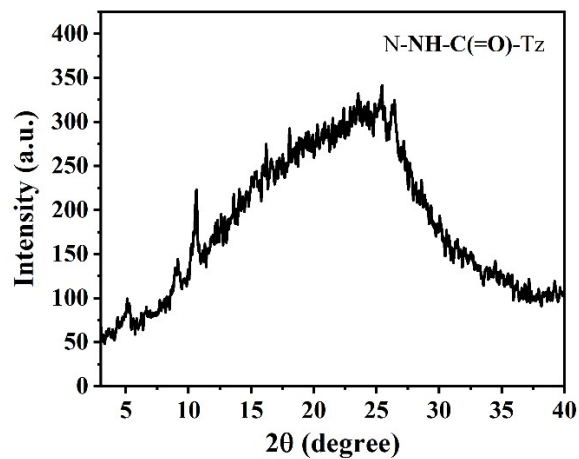


Figure S6. PXRD patterns of N-NH-C(=O)-Tz.

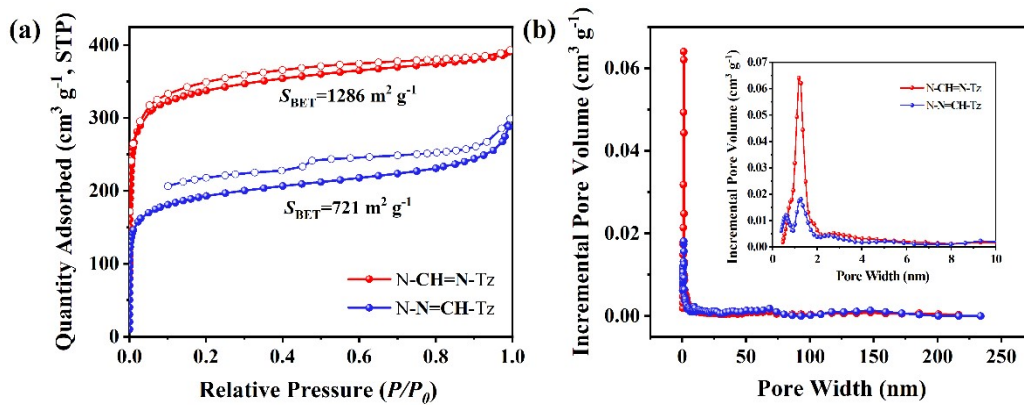


Figure S7. N₂ sorption isotherms (a) and pore size distributions (b) of N-CH=N-Tz and N-N=CH-Tz.

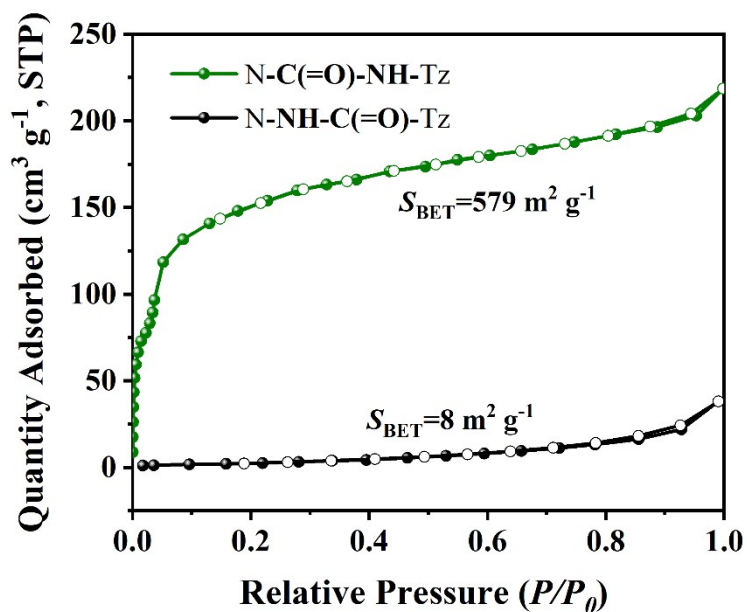


Figure S8. N₂ sorption isotherms of N-C(=O)-NH-Tz and N-NH-C(=O)-Tz.

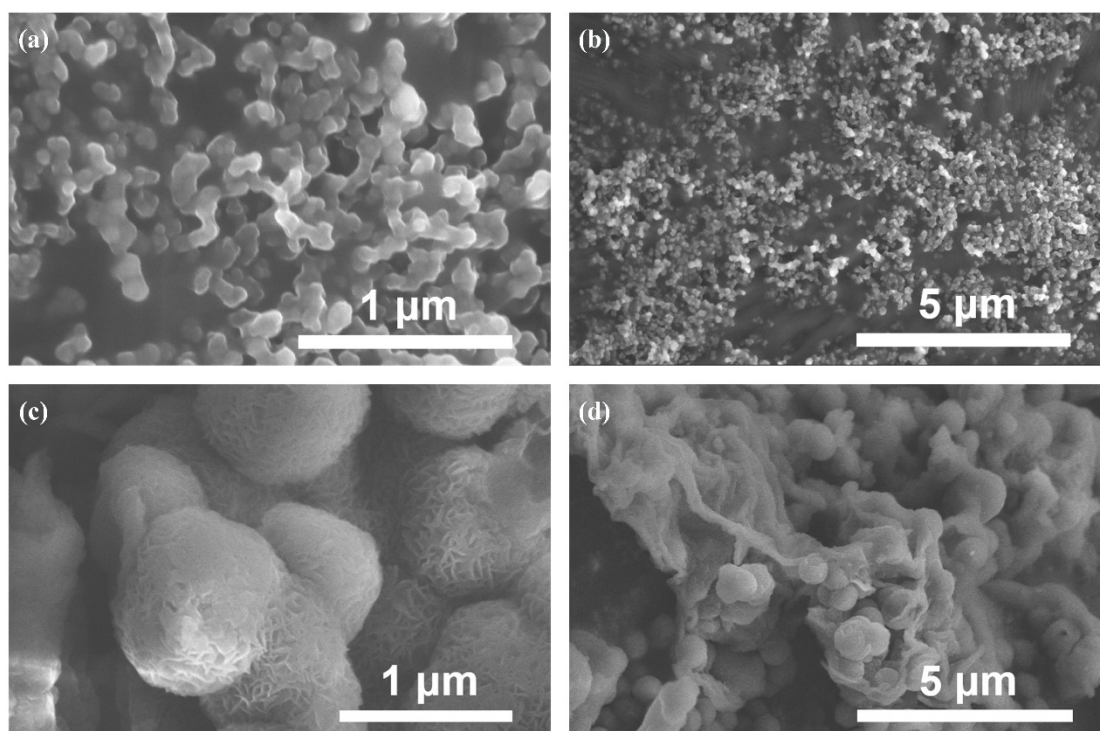


Figure S9. SEM images of N-CH=N-Tz (a, b) and N-N=CH-Tz (c, d).

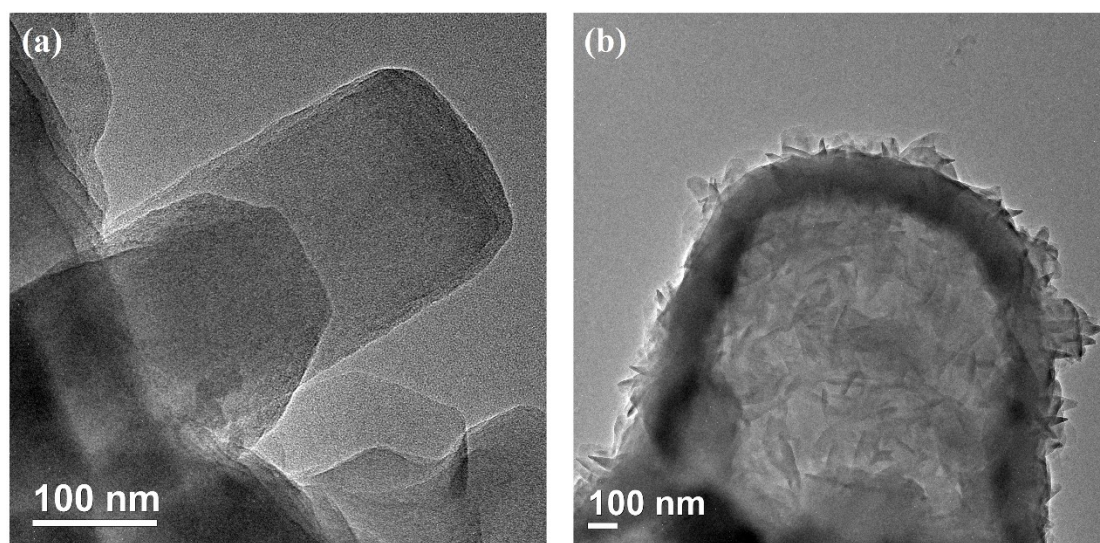


Figure S10. TEM images of N-CH=N-Tz (a) and N-N=CH-Tz (b).

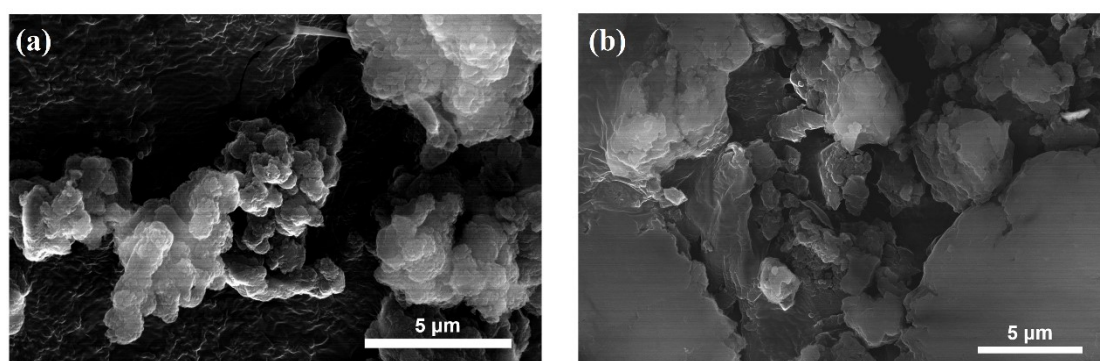


Figure S11. SEM images of N-C(=O)-NH-Tz (a) and N-NH-C(=O)-Tz (b).

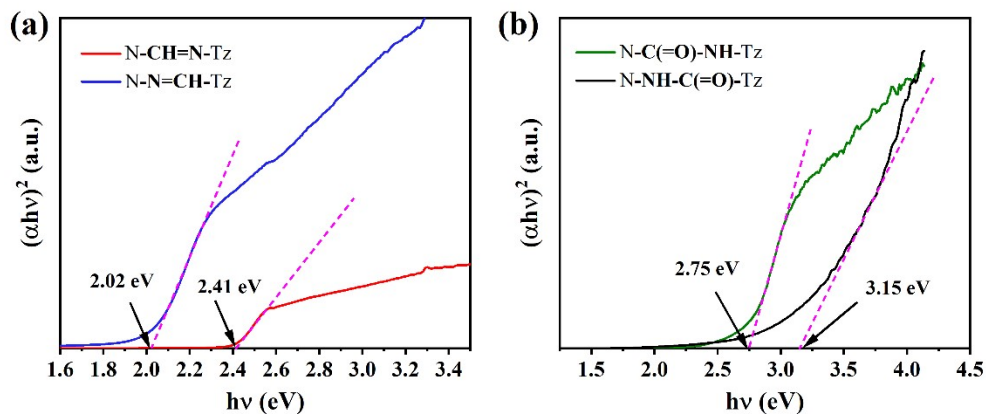


Figure S12. Tauc plot of N-CH=N-Tz and N-N=CH-Tz (b). Tauc plot of N-C(=O)-NH-Tz and N-NH-C(=O)-Tz (c).

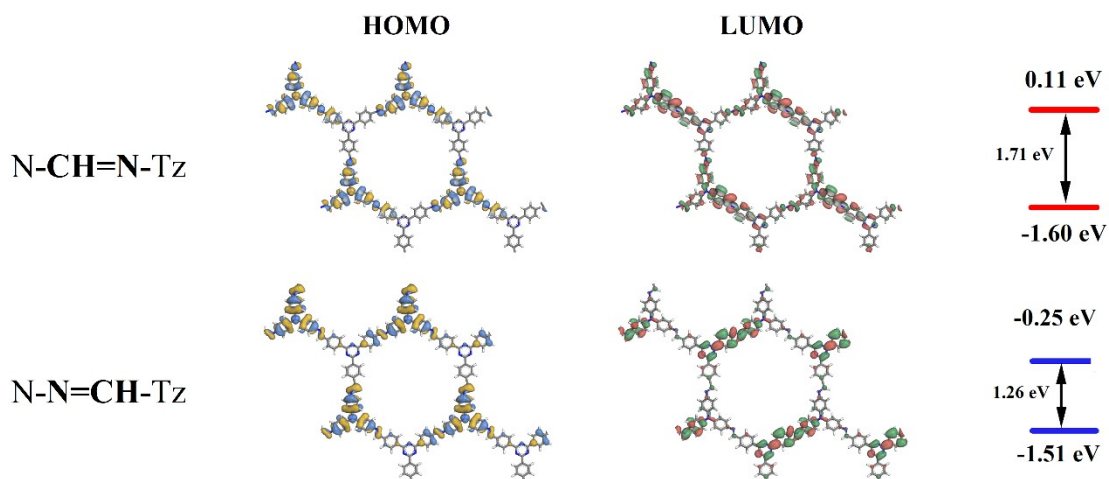


Figure S13. Structure units' electron distributions both in HOMO/LUMO states of N-CH=N-Tz and N-N=CH-Tz.

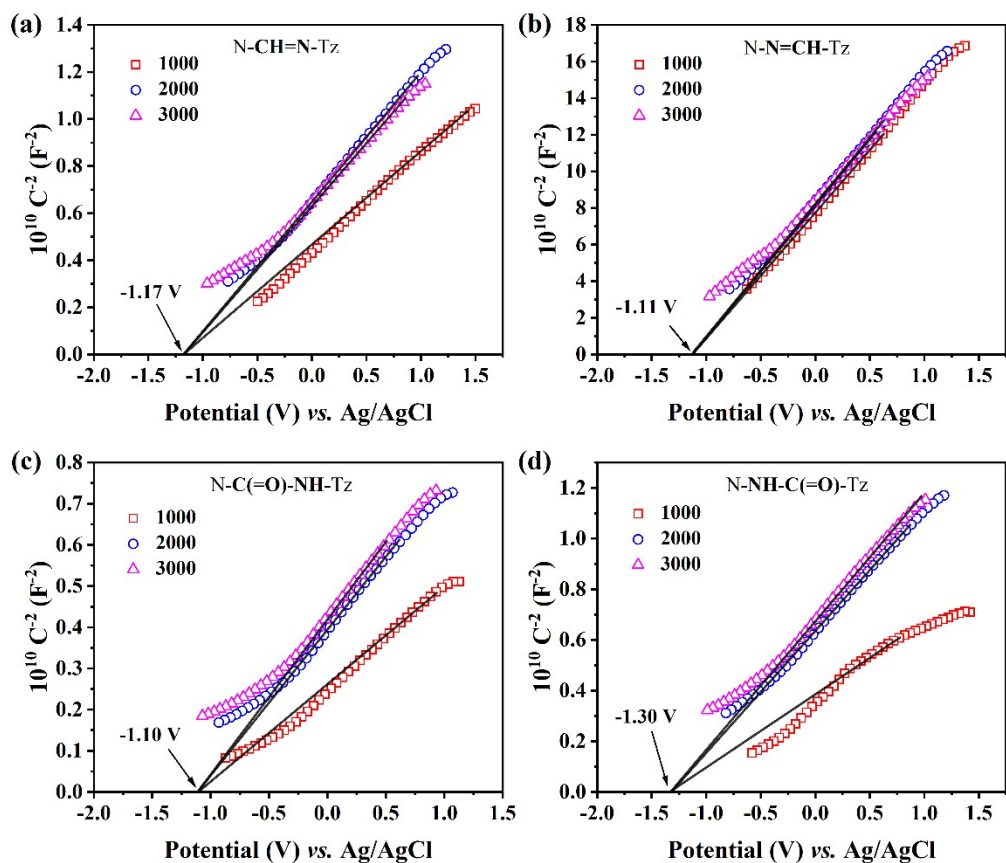


Figure S14. Mott-Schottky plots for N-CH=N-Tz (a), N-N=CH-Tz (b), N-C(=O)-NH-Tz (c) and N-NH-C(=O)-Tz (d) in 0.5 M Na_2SO_4 aqueous solution.

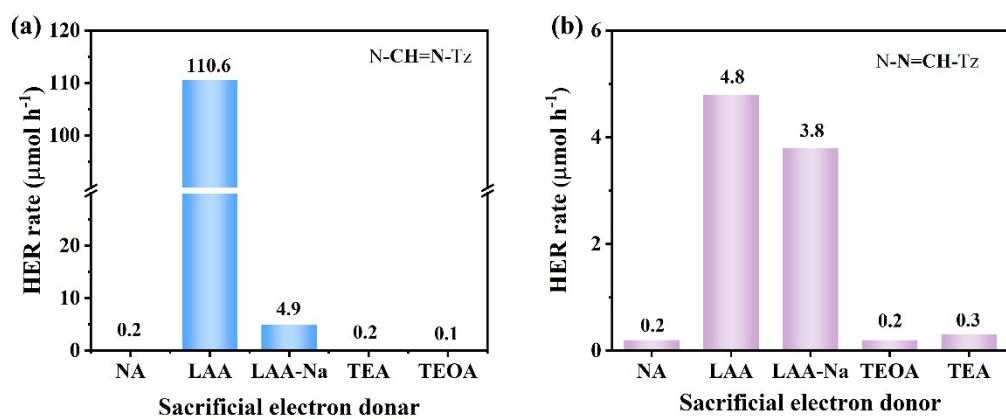


Figure S15. Screening of sacrificial electron donor of N-CH=N-Tz (a) and N-N=CH-Tz (b).

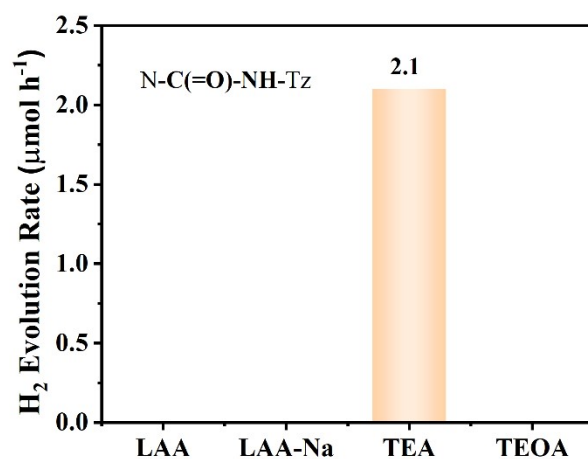


Figure S16. Screening of sacrificial electron donor of N-C(=O)-NH-Tz.

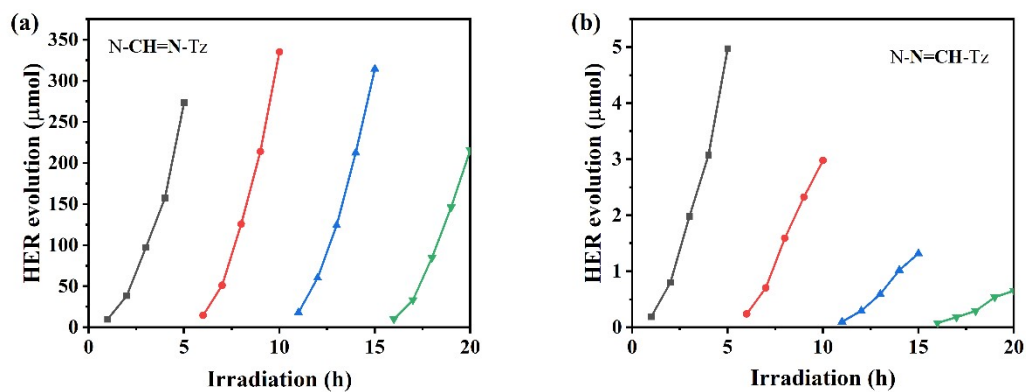


Figure S17. Recyclability test of imine COFs for 4 cycles over 20 h under visible light irradiation ($\lambda > 420$ nm) using LAA as a sacrificial agent.

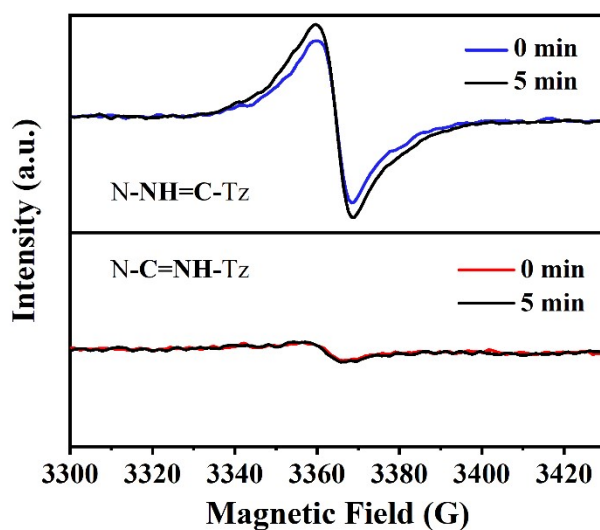


Figure S18. Room-temperature EPR spectra under dark and light conditions of N-CH=N-Tz and N-N=CH-Tz.

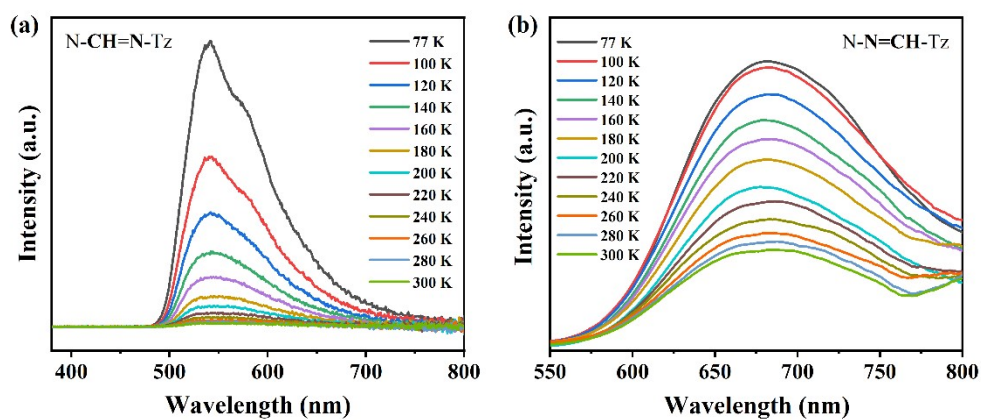


Figure S19. Temperature-dependent PL spectra with excitation wavelength at 360 nm of N-CH=N-Tz and N-N=CH-Tz.

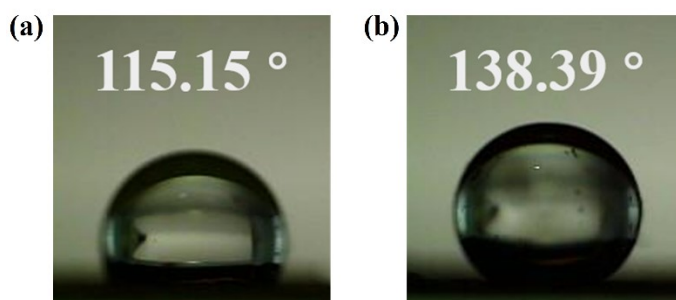


Figure S20. Water contact angle images of N-CH=N-Tz (a) and N-N=CH-Tz (b).

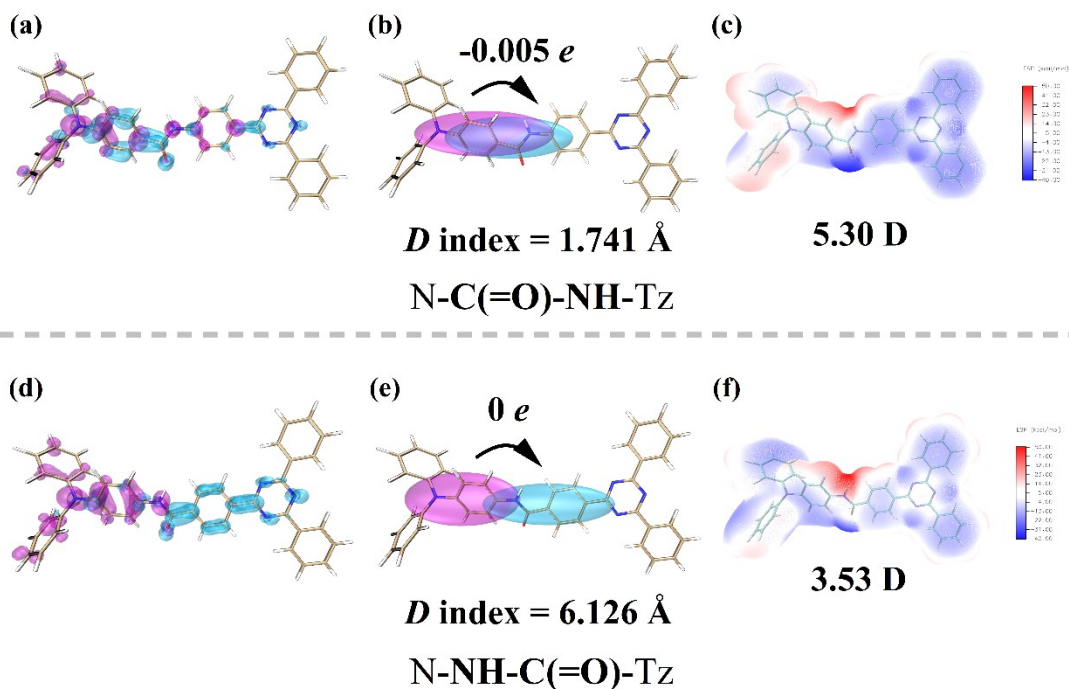


Figure S21. The hole (magenta) and electron (cyan) distribution of S1 excited states of N-C(=O)-NH-Tz (a, b) and N-NH-C(=O)-Tz (d, e). Electrostatic potential diagrams and dipole moments of N-C(=O)-NH-Tz (c) and N-NH-C(=O)-Tz (f).

Table S1. S_m and S_r index of isomeric materials

Materials	S_m	S_r
N-CH=N-Tz	0.44433	0.73902
N-N=CH-Tz	0.38987	0.69305
N-C(=O)-NH-Tz	0.43854	0.72846
N-NH-C(=O)-Tz	0.27071	0.56248

Table S2. Atomistic coordinates for AA-stacking mode of N-CH=N-Tz optimized using DMOL3 method (space group $P3$, $a = b = 22.8898 \text{ \AA}$, $c = 3.4205 \text{ \AA}$, $\alpha = \beta = 90^\circ$ and $\gamma = 120^\circ$).

<i>Atom</i>	<i>x/a</i>	<i>y/b</i>	<i>z/c</i>
C	0.50335	0.55568	0.40761
N	0.4887	0.50272	0.57285
C	0.52701	0.47087	0.59059
C	0.59338	0.50185	0.49719
C	0.62814	0.46821	0.51714
C	0.59732	0.40309	0.62989
C	0.53139	0.37278	0.72876
C	0.49694	0.40675	0.7115
C	0.63351	0.36674	0.63953
N	0.69987	0.39949	0.63918
C	0.45952	0.58354	0.41286
C	0.39858	0.55127	0.57238
C	0.35768	0.57837	0.57227
C	0.37624	0.63845	0.41487

C	0.4377	0.67025	0.25687
C	0.47873	0.6433	0.25494
H	0.6189	0.55191	0.41149
H	0.67892	0.49265	0.43955
H	0.5068	0.32297	0.82125
H	0.44629	0.38309	0.78964
H	0.38268	0.50505	0.69731
H	0.45471	0.71658	0.13828
H	0.52552	0.66915	0.12911
H	0.24056	0.68898	0.69132
H	0.54719	1.5798	0.25767
N	0.33333	0.66667	0.41518

Table S3. Atomistic coordinates for AA-stacking mode of N-N=CH-Tz optimized using DMOI3 method (space group $P3$, $a = b = 21.8594 \text{ \AA}$, $c = 3.7489 \text{ \AA}$, $\alpha = \beta = 90^\circ$ and $\gamma = 120^\circ$).

<i>Atom</i>	<i>x/a</i>	<i>y/b</i>	<i>z/c</i>
N	0.49353	0.54843	0.49904
C	0.46946	0.48513	0.50526
C	0.51185	0.45547	0.51356
C	0.58076	0.49341	0.51904
C	0.61898	0.46362	0.52243
C	0.58999	0.39492	0.52083
C	0.5212	0.35701	0.51661
C	0.48296	0.3867	0.51295
C	0.63065	0.36249	0.52218
N	0.69692	0.40102	0.52222
C	0.4506	0.57448	0.49585
C	0.38805	0.54381	0.65375

C	0.3501	0.57392	0.65519
C	0.37252	0.63577	0.49739
C	0.43523	0.66641	0.34074
C	0.47355	0.6368	0.3439
H	0.60401	0.54712	0.51972
H	0.67275	0.4937	0.52596
H	0.49797	0.30329	0.51546
H	0.42919	0.35617	0.50891
H	0.36928	0.49631	0.7867
H	0.4544	0.71442	0.21423
H	0.52195	0.66162	0.21743
H	0.24694	0.69793	0.78503
H	1.03436	1.58486	0.49776
N	0.33333	0.66667	0.49873

Reference

1. L. Grunenberg, G. Savasci, M. W. Terban, V. Duppel, I. Moudrakovski, M. Etter, R. E. Dinnebier, C. Ochsenfeld and B. V. Lotsch, Amine-Linked Covalent Organic Frameworks as a Platform for Postsynthetic Structure Interconversion and Pore-Wall Modification, *J. Am. Chem. Soc.*, 2021, **143**, 3430-3438.
2. Y.-X. Wang and M.-k. Leung, 4,4',4''-Tris(acetoxymethylene)triphenylamine: An Efficient Photoacid Promoted Chemical Cross-Linker for Polyvinylcarbazole and Its Applications for Photolithographic Hole-Transport Materials, *Macromolecules*, 2011, **44**, 8771-8779.
3. Z. Liu, Q. Su, P. Ju, X. Li, G. Li, Q. Wu and B. Yang, A Hydrophilic Covalent Organic Framework for Photocatalytic Oxidation of Benzylamine in Water, *Chem. Commun.*, 2020, **56**, 766-769.
4. K. Wu, Y. Du, H. Tang, Z. Chen and T. Lian, Efficient Extraction of Trapped Holes from Colloidal CdS Nanorods, *J. Am. Chem. Soc.*, 2015, **137**, 10224-10230.
5. <https://imagej.nih.gov/ij/plugins/contact-angle.html>.
6. B. Delley, An all-Electron Numerical Method for Solving the Local Density Functional for Polyatomic Molecules, *J. Chem. Phys.*, 1990, **92**, 508-517.
7. B. Delley, From Molecules to Solids with the DMol3 Approach, *J. Chem. Phys.*, 2000, **113**, 7756-7764.
8. R. A. Gaussian 09, M. J. Frisch, G. W. Trucks, H. B. Schlegel, G. E. Scuseria, J. R. C. M. A. Robb, G. Scalmani, V. Barone, B. Mennucci, G. A. Petersson, H. Nakatsuji, M. Caricato, X.

- Li, H. P. Hratchian, A. F. Izmaylov, J. Bloino, G. Zheng, J. L. Sonnenberg, M. Hada, M. Ehara, K. Toyota, R. Fukuda, J. Hasegawa, M. Ishida, T. Nakajima, Y. Honda, O. Kitao, H. Nakai, T. Vreven, J. A. Montgomery, Jr., J. E. Peralta, F. Ogliaro, M. Bearpark, J. J. Heyd, E. Brothers, K. N. Kudin, V. N. Staroverov, R. Kobayashi, J. Normand, K. Raghavachari, A. Rendell, J. C. Burant, S. S. Iyengar, J. Tomasi, and N. R. M. Cossi, J. M. Millam, M. Klene, J. E. Knox, J. B. Cross, V. Bakken, C. Adamo, J. Jaramillo, R. Gomperts, R. E. Stratmann, O. Yazyev, A. J. Austin, R. Cammi, C. Pomelli, J. W. Ochterski, R. L. Martin, K. Morokuma, V. G. Zakrzewski, G. A. Voth, P. Salvador, J. J. Dannenberg, S. Dapprich, A. D. Daniels, O. Farkas, J. B. Foresman, J. V. Ortiz, J. Cioslowski, and D. J. Fox., Gaussian 09, Revision A.01, *Gaussian, Inc., Wallingford CT*, 2009.
9. T. Lu and F. Chen, Multiwfn: A Multifunctional Wavefunction Analyzer, *J. Comput. Chem.*, 2012, **33**, 580-592.
 10. W. Zhao, P. Yan, H. Yang, M. Bahri, A. M. James, H. Chen, L. Liu, B. Li, Z. Pang, R. Clowes, N. D. Browning, J. W. Ward, Y. Wu and A. I. Cooper, Using Sound to Synthesize Covalent Organic Frameworks in Water, *Nat Synth*, 2022, **1**, 87-95.
 11. A. F. M. El-Mahdy, C.-H. Kuo, A. Alshehri, C. Young, Y. Yamauchi, J. Kim and S.-W. Kuo, Strategic Design of Triphenylamine- and Triphenyltriazine-Based Two-Dimensional Covalent Organic Frameworks for CO₂ Uptake and Energy Storage, *J. Mater. Chem. A*, 2018, **6**, 19532-19541.